Nonlinear Analysis: Modelling and Control, Online First, 1–19
https://doi.org/10.15388/namc.2025.30.38975

Vilnius University Press

Mitigating atmospheric carbon dioxide through deployment of renewable energy: A mathematical model

Anjali Jha, Arvind Kumar Misra[1]

Department of Mathematics, Institute of Science,
Banaras Hindu University,
Varanasi – 221 005, India
anjalijha1895@gmail.com; akmisra@bhu.ac.in

Received: April 19, 2024 / **Revised:** January 23, 2025 / **Published online:** March 3, 2025

Abstract. In recent decades, the widespread reliance on fossil fuels has grown substantially, leading to a rise in atmospheric carbon dioxide (CO_2), which poses a major global concern. In this study, we develop and analyze a novel mathematical model to examine the interactions between atmospheric CO_2, human population, and energy demand. The model assumes that human activities and energy production from traditional sources (oil, coal, and gas) contribute to increasing CO_2 level, while a shift in energy dependence from traditional to renewable sources (hydro, solar, etc.) occurs as a result of environmental awareness. We derive sufficient conditions for both local and global stability of the system's interior equilibrium. Numerical simulations demonstrate that when reliance on renewable energy sources is low, the system can exhibit oscillatory dynamics and various bifurcations. However, beyond a critical threshold of renewable energy dependency, the system stabilizes around the interior equilibrium, leading to a reduction in atmospheric CO_2. Additionally, an optimal control problem is formulated to reduce atmospheric CO_2 level while minimizing the associated implementation costs.

Keywords: carbon dioxide, energy, Lyapunov's stability, optimal control.

1 Introduction

Energy serves as the driving force behind human life and stands as a cornerstone of continuous progress. As civilization advances, the global demand for energy surges, driven by factors such as population growth, urbanization, and modernization [25]. Currently, fossil fuels satisfy approximately 80% of the world's energy requirements [17, 32]. These hydrocarbons, formed by buried organisms, release CO_2 when burned, imposing detrimental effects on the planet. Human-induced CO_2 emissions directly imperil the environment, contributing to approximately 160,000 annual deaths resulting from floods, droughts, and diseases like malaria, malnutrition, and diarrhea [30]. The IPCC warns that if current CO_2 accumulation trends persist, the global average surface temperature could

[1]Corresponding author.

increase by 2 °C by 2100, directly impacting human population, species, and intensifying wildfires [15].

Recognizing the environmental impacts of fossil fuel burning, governments and policymakers worldwide champion renewable energy sources as viable alternatives [26]. Renewable energy, harnessed from natural sources such as sunlight and gravity and transformed into usable energy through various technologies, offers a sustainable solution with minimal environmental impact compared to traditional sources [2, 6, 23]. Research in the United States by Bull [3] demonstrates that adopting renewable energy for electricity generation annually averts approximately 70 million metric tons of CO_2 emissions. Studies also suggest that combining different renewable energy resources would significantly contribute to ensuring pollution free energy [1]. According to a report from IRENA [31], meeting the Paris Climate goal of keeping global warming well below 2 °C requires completely eliminating CO_2 emissions from energy production by 2050. The report emphasizes the importance of renewable energy growth, stating that in 2015, 19% of the world's final energy demand was met by renewable sources, with an annual increase of 0.17% since 2010.

In past few years, numerous studies have been conducted to examine the effects of various factors such as human population, environmental taxes, among other measures, on atmospheric CO_2 level [8, 20–22, 24, 27, 29]. Misra and Verma have investigated the role of environmental education in reducing anthropogenic CO_2 emissions [22], concluding that if the educated population achieves only minimal reductions in their carbon footprint, increasing the implementation rate of educational programs has a limited impact on controlling atmospheric CO_2 level. Fan et al. [8] studied the impact of environmental taxes on greenhouse gas level and suggested that implementing such taxes, alongside strict government measures to combat corruption, could effectively improve environmental quality. Verma et al. [29] have studied a model to suggest a strategy for optimal reduction of energy-related emissions of CO_2. They have concluded that increasing highly efficient technologies and low carbon energy sources might cut down CO_2 emission and also reduce mitigation cost. Tiwari et al. [27] have developed a nonautonomous mathematical model designed to reduce atmospheric CO_2 using algae biomass. The model suggests that continuously introducing algae into the ocean can help lower atmospheric CO_2 level. Further, Nadeem et al. [24] have formulated and analyzed a fractional mathematical model using Caputo fractional derivative for climate change and developed a numerical scheme to obtain an optimal solution. By formulating a mathematical model, Misra and Jha [21] calculated the amount of cleared land needed for planting leafy trees to restore atmospheric CO_2 level to their preclearance state.

The widespread adoption of renewable energy holds the potential to reduce CO_2 emissions stemming from energy production. Policymakers in various nations such as China, the USA, India, Germany are actively discussing strategies to curb CO_2 emissions by shifting to clean energy. In this study, we develop an ODE mathematical model to analyze the impact of deploying clean energy on future atmospheric CO_2 concentration. Our model considers that the human population currently utilizes both traditional and renewable energy sources to meet their energy needs. But as the atmospheric CO_2 level rises, it affects the human population negatively, which motivate them to shift towards

renewable energy sources to meet their energy demands. This study uniquely develops a nonlinear mathematical model to evaluate the impact of transitioning from traditional to renewable energy sources on future atmospheric CO_2 level. Unlike earlier models, we incorporate the feedback mechanism where rising CO_2 level negatively affect the population, which, in turn, motivates the human population to shift towards renewable energy. This dynamic interaction has not been comprehensively analyzed in prior researches. Furthermore, our study highlights the challenges of adopting renewable energy and provides insights into its potential effectiveness, offering a novel perspective for policymakers.

2 Mathematical model

For the model formulation, we take into account four dynamical variables, namely atmospheric concentration of CO_2 ($C(t)$), human population ($N(t)$), demand of traditional energy ($E_{\mathrm{ts}}(t)$), and renewable energy ($E_{\mathrm{os}}(t)$).

In the preindustrial era, the atmospheric CO_2 level remained relatively stable at a constant value, C_0. However, human activities, including fossil fuel combustion and land-use changes, have caused an increase in CO_2 concentrations [11]. Anthropogenic CO_2 emissions, apart from those releasing from fossil fuel burning, are directly related to the human population N represented by the term $\lambda_1 N$. Additionally, CO_2 emissions resulting from fossil fuel combustion are linked to the demand for traditional energy sources denoted by the term $\lambda_2 E_{\mathrm{ts}}$. The human population experiences logistic growth characterized as $sN(1 - N/L)$. The rising atmospheric CO_2 concentration adversely affects the human population. These negative effects, stemming from the increase in CO_2 level from the preindustrial era, result in heightened frequency and intensity of natural disasters, reduced rainfall in subtropical regions, scarcity of drinking water sources, higher occurrences of vector-borne diseases, malnutrition, and fatalities due to heat waves [10]. The adverse effects cause the human population to decrease at a rate $\theta(C - C_0)N$. Energy is essential for human survival, highlighting the critical need for a secure and accessible energy supply in modern societies' sustainability. However, our heavy reliance on fossil fuels faces significant challenges like dwindling reserves and growing environmental concerns. In response to this complex scenario, renewable energy emerges as a promising and definitive solution to these challenges. Regarding the growth of energy demand, it is mentioned in a study [12] that the sources of energy follow logistic growth. The increasing population drives higher energy requirements, which can be fulfilled either by the renewable sources or the traditional energy sources. Therefore, we propose a strategic approach: a fraction of the energy demand (γ) is met by renewable sources with the remaining portion $(1 - \gamma)$ fulfilled by conventional energy sources. As the energy demand of human population has a upper ceiling, for the model formulation, we incorporate the Holling type-II functional response for the growth of energy demand, providing depth to our understanding of the delicate balance between human needs and available energy resources. Therefore, the system of differential equations governing the interaction between the atmospheric CO_2 level, human population, demand of traditional and renewable energy sources according

to above considerations is given as follows:

$$\begin{aligned}
\frac{\mathrm{d}C}{\mathrm{d}t} &= -\alpha(C - C_0) + \lambda_1 N + \lambda_2 E_{\mathrm{ts}},\\
\frac{\mathrm{d}N}{\mathrm{d}t} &= sN\left(1 - \frac{N}{L}\right) - \theta(C - C_0)N + \beta N\big((1-\gamma)E_{\mathrm{ts}} + \gamma E_{\mathrm{os}}\big),\\
\frac{\mathrm{d}E_{\mathrm{ts}}}{\mathrm{d}t} &= \frac{k_1(1-\gamma)NE_{\mathrm{ts}}}{m+N} - \gamma_{\mathrm{ts}}E_{\mathrm{ts}}^2, \qquad \frac{\mathrm{d}E_{\mathrm{os}}}{\mathrm{d}t} = \frac{k_2\gamma NE_{\mathrm{os}}}{m+N} - \gamma_{\mathrm{os}}E_{\mathrm{os}}^2
\end{aligned} \tag{1}$$

with $C(0) \geqslant C_0$, $N(0) \geqslant 0$, $E_{\mathrm{ts}}(0) \geqslant 0$, and $E_{\mathrm{os}}(0) \geqslant 0$. Here β, γ, γ_{ts}, and γ_{os} are the growth rate coefficient of human population due to energy, fraction of energy produced through renewable energy sources, depletion rate coefficients of demand for traditional and renewable energies due to their limited amount, respectively. Traditional energy sources are finite, so energy production from these sources peaks and then declines. Further, the production of renewable energy tends to grow for a long term, then decline. Therefore, we have represented this depletion as density-dependent to show that energy demand diminishes over time because of the limited availability of resources. Moreover, m, k_1, and k_2 are half-saturation constant of the demand for energy, growth rate coefficients of demand for energy from traditional and renewable energy sources, respectively.

Region of attraction for the formulated model system (1) is contained in Ω, [9, 18]

$$\Omega = \left\{(C, N, E_{\mathrm{ts}}, E_{\mathrm{os}}) \in \mathbb{R}_+^4 \colon C_0 \leqslant C \leqslant \frac{\lambda_1 N_m + \lambda_2 E_{ts_m}}{\alpha}, \right.$$
$$\left. 0 \leqslant N \leqslant N_m, 0 \leqslant E_{\mathrm{ts}} \leqslant E_{ts_m},\ 0 \leqslant E_{\mathrm{os}} \leqslant \frac{k_2\gamma}{\gamma_{\mathrm{os}}}\right\},$$

where

$$N_m = \frac{L}{s}\left[s + \beta\left\{\frac{k_1(1-\gamma)^2}{\gamma_{\mathrm{ts}}} + \frac{k_2\gamma^2}{\gamma_{\mathrm{os}}}\right\}\right] \quad \text{and} \quad E_{ts_m} = \frac{k_1(1-\gamma)}{\gamma_{\mathrm{ts}}}.$$

3 Model analysis

The proposed model is nonlinear, making it challenging to derive an analytical solution. Consequently, a qualitative analysis is conducted. Initially, the feasible equilibrium points of the model system (1) are determined, followed by an examination of their stability properties.

3.1 Equilibrium analysis

Equilibrium points representing the steady-state solutions of system (1) are determined by equating the right-hand side of Eq. (1) to zero. For the proposed model system (1), the following feasible equilibrium points have been identified:

(i) $E_0(C_0, 0, 0, 0)$. In this equilibrium the dynamic variable N is zero, and hence E_{ts} and E_{os} are zero.

(ii) $E_1(C_0 + \lambda_1 sL/(\alpha s + \lambda_1 \theta L), \alpha sL/(\alpha s + \lambda_1 \theta L), 0, 0)$. In this equilibrium the demand for energy by the human population is zero.
(iii) $E_2(C_2, N_2, E_{ts_2}, 0)$. In this equilibrium, $E_{\rm os}$ is zero.
(iv) $E_3(C_3, N_3, 0, E_{os_3})$. In this equilibrium, $E_{\rm ts}$ is zero.
(v) $E^*(C^*, N^*, E^*_{\rm ts}, E^*_{\rm os})$. In this equilibrium all the considered dynamical variables coexist.

Equilibria E_0 and E_1 can be easily obtained. Equilibrium E_2 can be given as the positive solution of the following algebraic equations:

$$-\alpha(C - C_0) + \lambda_1 N + \lambda_2 E_{\rm ts} = 0, \tag{2}$$

$$s\left(1 - \frac{N}{L}\right) - \theta(C - C_0) + \beta(1 - \gamma)E_{\rm ts} = 0, \tag{3}$$

$$\frac{k_1(1 - \gamma)N}{m + N} - \gamma_{\rm ts} E_{\rm ts} = 0. \tag{4}$$

From Eqs. (4) and (2) we get

$$E_{\rm ts} = \frac{k_1(1 - \gamma)N}{\gamma_{\rm ts}(m + N)} \quad \text{and} \quad C = C_0 + \frac{1}{\alpha}\left(\lambda_1 N + \frac{\lambda_2 k_1(1 - \gamma)N}{\gamma_{\rm ts}(m + N)}\right).$$

Putting these values of C and $E_{\rm ts}$ in Eq. (3), we get a quadratic equation in N as

$$\begin{aligned}&\gamma_{\rm ts}(s\alpha + \lambda_1\theta L)N^2 + \big[s\gamma_{\rm ts}\alpha m - s\gamma_{\rm ts}\alpha L - \beta(1 - \gamma)^2 k_1 L\alpha \\ &\quad + \theta L\lambda_1\gamma_{\rm ts} m + \theta L\lambda_2 k_1(1 - \gamma)\big]N - s\gamma_{\rm ts}\alpha L m = 0,\end{aligned}$$

which has a unique positive root. Obtaining a positive root for N (denoted as N_2), we can determine the corresponding positive values of C and $E_{\rm ts}$ (say C_2 and E_{ts_2}), and thus equilibrium $E_2(C_2, N_2, E_{ts_2}, 0)$ is obtained.

Equilibrium E_3 can be given as the positive solution of the following algebraic equations:

$$-\alpha(C - C_0) + \lambda_1 N = 0, \tag{5}$$

$$s\left(1 - \frac{N}{L}\right) - \theta(C - C_0) + \beta\gamma E_{\rm os} = 0, \tag{6}$$

$$\frac{k_2\gamma N}{m + N} - \gamma_{\rm os} E_{\rm os} = 0. \tag{7}$$

From Eq. (7) $E_{\rm os} = k_2\gamma N/(\gamma_{\rm os}(m + N))$, and Eq. (5) gives $C = C_0 + \lambda_1 N/\alpha$. Putting these values of C and $E_{\rm os}$ in Eq. (6), we get a quadratic equation in N as

$$\begin{aligned}&\gamma_{\rm os}(s\alpha + \lambda_1\theta L)N^2 + \big[\gamma_{\rm os} m(s\alpha + \lambda_1\theta L) - s\alpha\gamma_{\rm os} L - \beta\gamma^2 k_2 L\alpha\big]N \\ &\quad - s\alpha\gamma_{\rm os} L m = 0,\end{aligned}$$

which has a unique positive root. Obtaining a positive root for N (denoted as N_3), we can determine the corresponding positive values of C and $E_{\rm ts}$ (say C_3 and E_{os_3}), and thus equilibrium $E_3(C_3, N_3, 0, E_{os_3})$ is obtained.

Equilibrium E^* is given as the positive solution of the following algebraic equations:

$$-\alpha(C - C_0) + \lambda_1 N + \lambda_2 E_{\rm ts} = 0, \tag{8}$$

$$s\left(1 - \frac{N}{L}\right) - \theta(C - C_0) + \beta\big[(1-\gamma)E_{\rm ts} + \gamma E_{\rm os}\big] = 0, \tag{9}$$

$$\frac{k_1(1-\gamma)N}{m+N} - \gamma_{\rm ts}E_{\rm ts} = 0, \qquad \frac{k_2\gamma N}{m+N} - \gamma_{\rm os}E_{\rm os} = 0. \tag{10}$$

From Eqs. (10) $E_{\rm ts} = k_1(1-\gamma)N/(\gamma_{\rm ts}(m+N))$ and $E_{\rm os} = k_2\gamma N/(\gamma_{\rm os}(m+N))$. Further, Eq. (8) gives $C = C_0 + (\lambda_1 N + \lambda_2 k_1(1-\gamma)N/(\gamma_{\rm ts}(m+N)))/\alpha$. Putting these values of C, $E_{\rm ts}$, and $E_{\rm os}$ in Eq. (9), we get a quadratic equation in N as

$$\tilde{p}_1 N^2 + \tilde{p}_2 N - \tilde{p}_3 = 0, \tag{11}$$

here

$$\begin{aligned}
\tilde{p}_1 &= \gamma_{\rm ts}\gamma_{\rm os}(s\alpha + \lambda_1\theta L),\\
\tilde{p}_2 &= \big[(s\alpha + \lambda_1\theta L)\gamma_{\rm ts}\gamma_{\rm os}m - s\gamma_{\rm ts}\alpha\gamma_{\rm os}L + \beta L\alpha k_1\gamma_{\rm os}(1-\gamma)^2\\
&\quad - \beta L\alpha\gamma^2 k_2\gamma_{\rm ts} + \theta L\gamma_{\rm os}\lambda_2 k_1(1-\gamma)\big],\\
\tilde{p}_3 &= s\gamma_{\rm ts}\alpha\gamma_{\rm os}Lm.
\end{aligned}$$

Equation (11) has a unique positive root. Obtaining a positive root for N, we get the positive values of C, $E_{\rm ts}$, and $E_{\rm os}$, and thus the interior equilibrium $E^*(C^*, N^*, E^*_{\rm ts}, E^*_{\rm os})$ is obtained.

3.2 Stability analysis

Stability analysis of an equilibrium is performed to determine whether the solution trajectories of formulated system settle to the equilibrium or repel from its neighborhood. The local stability of equilibrium depicts the behavior of equilibrium around its small neighborhood, and in global stability, the whole region of attraction is considered.

We perform a local stability analysis of the feasible equilibrium points by examining the eigenvalues of the Jacobian matrix for boundary equilibria [19] and applying Lyapunov stability theory for the interior equilibrium [13]. The Jacobian matrix for the formulated system (1) is given as follows:

$$P = \begin{pmatrix}
-\alpha & \lambda_1 & \lambda_2 & 0\\
-\theta N & a_{22} & \beta(1-\gamma)N & \beta\gamma N\\
0 & \frac{k_1(1-\gamma)mE_{\rm ts}}{(m+N)^2} & \frac{k_1(1-\gamma)N}{m+N} - 2\gamma_{\rm ts}E_{\rm ts} & 0\\
0 & \frac{k_2\gamma mE_{\rm os}}{(m+N)^2} & 0 & \frac{k_2\gamma N}{m+N} - 2\gamma_{\rm os}E_{\rm os}
\end{pmatrix},$$

where $a_{22} = s(1-2N/L) - \theta(C - C_0) + \beta((1-\gamma)E_{\rm ts} + \gamma E_{\rm os})$. The Jacobian matrix at E_0 has one eigenvalue s, which is always positive, hence the equilibrium E_0 is always unstable. The Jacobian matrix at E_1 has two eigenvalues $k_1(1-\gamma)N_1/(m+N_1)$ and $k_2\gamma N_1/(m+N_1)$, where $N_1 = \alpha sL/(\alpha s + \lambda_1\theta L)$, and these eigenvalues are always

positive, hence the equilibrium E_1 is always unstable. The Jacobian matrix at E_2 and E_3 have eigenvalues $k_2\gamma N_2/(m+N_2)$ and $k_1(1-\gamma)N_3/(m+N_3)$, respectively, which are always positive, hence the equilibria E_2 and E_3 are always unstable. The following Theorem 1 presents the sufficient conditions under which the interior equilibrium E^* is locally stable.

Theorem 1. *Under the following conditions, equilibrium E^* is locally stable*:

$$\max\left\{\frac{3\lambda_2^2}{4\alpha\gamma_{\rm ts}}, \frac{3\lambda_1 L\beta^2(1-\gamma)^2}{\theta s}\right\} < \frac{\lambda_1 s\gamma_{\rm ts}^2(m+N^*)^4}{m^2k_1^2(1-\gamma)^2\theta L} \quad \textit{and} \quad \beta\gamma^2 < \frac{s\gamma_{\rm os}(m+N^*)^2}{mk_2L}.$$

Proof. We begin by linearizing system (1) around the interior equilibrium E^* using the following transformations:

$$\begin{aligned} C &= C^* + \tilde{u}_1, \qquad & E_{\rm ts} &= E_{\rm ts}^* + \tilde{u}_3,\\ N &= N^* + \tilde{u}_2, \qquad & E_{\rm os} &= E_{\rm os}^* + \tilde{u}_4, \end{aligned}$$

where $\tilde{u}_1$, $\tilde{u}_2$, $\tilde{u}_3$, and $\tilde{u}_4$ represent small perturbations. Next, we consider a Lyapunov function as follows:

$$V = \frac{1}{2}\left(\tilde{u}_1^2 + \frac{n_1}{N^*}\tilde{u}_2^2 + \frac{n_2}{E_{\rm ts}^*}\tilde{u}_3^2 + \frac{n_3}{E_{\rm os}^*}\tilde{u}_4^2\right).$$

Differentiating V concerning time t in relation to the solutions of the linearized system of (1) gives

$$\begin{aligned} \frac{{\rm d}V}{{\rm d}t} &= -\alpha\tilde{u}_1^2 - \frac{n_1 s}{L}\tilde{u}_2^2 - n_2\gamma_{\rm ts}\tilde{u}_3^2 - n_3\gamma_{\rm os}\tilde{u}_4^2\\ &\quad + (\lambda_1 - n_1\theta)\tilde{u}_1\tilde{u}_2 + \lambda_2\tilde{u}_1\tilde{u}_3 + n_1\beta(1-\gamma)\tilde{u}_2\tilde{u}_3 + n_1\beta\gamma\tilde{u}_2\tilde{u}_4\\ &\quad + \frac{n_2k_1(1-\gamma)m}{(m+N^*)^2}\tilde{u}_2\tilde{u}_3 + \frac{n_3k_2\gamma m}{(m+N^*)^2}\tilde{u}_2\tilde{u}_4. \end{aligned}$$

Choosing $n_1 = \lambda_1/\theta$, ${\rm d}V/{\rm d}t$ becomes negative definite provided:

$$\lambda_2^2 < \frac{4}{3}\alpha n_2\gamma_{\rm ts}, \qquad \left\{n_1\beta(1-\gamma)\right\}^2 < \frac{1}{3}\frac{n_1 s}{L}n_2\gamma_{\rm ts}, \qquad \left\{n_1\beta\gamma\right\}^2 < 2\frac{n_1 s}{L}n_3\gamma_{\rm os},$$
$$\left\{\frac{n_2k_1(1-\gamma)m}{(m+N^*)^2}\right\}^2 < \frac{1}{3}\frac{n_1 s}{L}n_2\gamma_{\rm ts}, \qquad \left\{\frac{n_3k_2\gamma m}{(m+N^*)^2}\right\}^2 < \frac{1}{2}\frac{n_1 s}{L}n_3\gamma_{\rm os}.$$

Using the chosen value of constant n_1, the above inequalities reduce to the inequalities mentioned in Theorem 1, where the constants n_2 and n_3 can be chosen from the first and second inequality of the mentioned inequalities, respectively. The inequalities mentioned in Theorem 1 are sufficient conditions for the local stability of E^*. □

Furthermore, we discuss about the nonlinear stability of E^* in the attracting region contained in the set Ω. For this, we apply the Lyapunov second method [5, 7].

Theorem 2. *Under the following conditions, equilibrium E^* is globally stable inside Ω:*

$$\max\left\{\frac{3\lambda_2^2}{4\alpha\gamma_{\rm ts}}, \frac{3\lambda_1 L\beta^2(1-\gamma)^2}{\theta s}\right\} < \frac{\lambda_1 s\gamma_{\rm ts}^2(m+N^*)^2}{k_1^2(1-\gamma)^2\theta L} \quad \textit{and} \quad \beta\gamma^2 < \frac{s\gamma_{\rm os}(m+N^*)}{k_2 L}.$$

Proof. Consider a positive definite function W as

$$W = \frac{1}{2}(C-C^*)^2 + m_1\left(N - N^* - N^*\ln\frac{N}{N^*}\right) + m_2\left(E_{\rm ts} - E_{\rm ts}^* - E_{\rm ts}^*\ln\frac{E_{\rm ts}}{E_{\rm ts}^*}\right) + m_3\left(E_{\rm os} - E_{\rm os}^* - E_{\rm os}^*\ln\frac{E_{\rm os}}{E_{\rm os}^*}\right).$$

Differentiating W concerning time t along the solution trajectories of model system (1), we have

$$\begin{aligned}\frac{{\rm d}W}{{\rm d}t} = {}& -\alpha(C-C^*)^2 - \frac{m_1 s}{L}(N-N^*)^2 \\ & - m_2\gamma_{\rm ts}(E_{\rm ts}-E_{\rm ts}^*)^2 - m_3\gamma_{\rm os}(E_{\rm os}-E_{\rm os}^*)^2 \\ & + (\lambda_1 - m_1\theta)(C-C^*)(N-N^*) + \lambda_2(C-C^*)(E_{\rm ts}-E_{\rm ts}^*) \\ & + m_1\beta\gamma(N-N^*)(E_{\rm os}-E_{\rm os}^*) + m_1\beta(1-\gamma)(N-N^*)(E_{\rm ts}-E_{\rm ts}^*) \\ & + \frac{m_2 k_1 m(1-\gamma)}{(m+N)(m+N^*)}(N-N^*)(E_{\rm ts}-E_{\rm ts}^*) \\ & + \frac{m_3 k_2\gamma m}{(m+N)(m+N^*)}(N-N^*)(E_{\rm os}-E_{\rm os}^*).\end{aligned}$$

Choosing $m_1 = \lambda_1/\theta$, ${\rm d}W/{\rm d}t$ becomes negative definite provided:

$$\lambda_2^2 < \frac{4}{3}\alpha m_2\gamma_{\rm ts}, \quad \left\{m_1\beta(1-\gamma)\right\}^2 < \frac{1}{3}\frac{m_1 s}{L}m_2\gamma_{\rm ts}, \quad \left\{m_1\beta\gamma\right\}^2 < 2\frac{m_1 s}{L}m_3\gamma_{\rm os},$$
$$\left\{\frac{m_2 k_1(1-\gamma)m}{(m+N)(m+N^*)}\right\}^2 < \frac{1}{3}\frac{m_1 s}{L}m_2\gamma_{\rm ts}, \quad \left\{\frac{m_3 k_2\gamma m}{(m+N)(m+N^*)}\right\}^2 < \frac{1}{2}\frac{m_1 s}{L}m_3\gamma_{\rm os}.$$

Using the chosen value of constant m_1, the above inequalities reduce to the inequalities mentioned in Theorem 2, where the constants m_2 and m_3 can be chosen from the first and second inequality of the mentioned inequalities, respectively. These are sufficient conditions for the global stability of E^* inside Ω. □

3.3 Optimal control

Through optimal control technique, a strategy can be determined for a dynamical system that optimizes the objective function with respect to some considered set of control parameters. In the past, some mathematical models have been analyzed using optimal control strategies for the mitigation of CO_2 [4, 28]. Using optimal control technique, we want to explore a strategy, which minimizes the atmospheric level of CO_2 along with minimizing

the cost involved in doing so. One of the most efficient way of minimizing the atmospheric level of CO_2 is increasing the dependency of human population on renewable sources of energy. Therefore, we have considered the fraction of dependency of human population on renewable energy sources as a control parameter and formulated objective functional to minimize the cost of implementation of this considered strategy. The parameter γ of system (1) is taken as a function of time, which is Lebesgue measurable, and hence system (1) takes the form

$$\begin{aligned}
&\frac{\mathrm{d}C}{\mathrm{d}t} = -\alpha(C - C_0) + \lambda_1 N + \lambda_2 E_{\mathrm{ts}},\\
&\frac{\mathrm{d}N}{\mathrm{d}t} = sN\left(1 - \frac{N}{L}\right) - \theta(C - C_0)N + \beta N\big(\big(1 - \gamma(t)\big)E_{\mathrm{ts}} + \gamma(t)E_{\mathrm{os}}\big),\\
&\frac{\mathrm{d}E_{\mathrm{ts}}}{\mathrm{d}t} = \frac{k_1(1 - \gamma(t))NE_{\mathrm{ts}}}{m + N} - \gamma_{\mathrm{ts}}E_{\mathrm{ts}}^2, \qquad \frac{\mathrm{d}E_{\mathrm{os}}}{\mathrm{d}t} = \frac{k_2\gamma(t)NE_{\mathrm{os}}}{m + N} - \gamma_{\mathrm{os}}E_{\mathrm{os}}^2,
\end{aligned} \tag{12}$$

where $C(0) \geqslant C_0$, $N(0) \geqslant 0$, $E_{\mathrm{ts}}(0) \geqslant 0$, and $E_{\mathrm{os}}(0) \geqslant 0$. Our aim here is to minimize the atmospheric level of CO_2 and the cost of implementation of this strategy. Therefore, the objective functional which we want to minimize is

$$J = \int_0^{t_f} \big[AC(t) + B\gamma^2(t)\big]\,\mathrm{d}t,$$

where A and B are positive weight constants.

3.4 Characterization of optimal control

Using the Pontryagin's maximum principle, we determine the necessary conditions for the control problem. The Hamiltonian for the control problem (12) is formulated as

$$\begin{aligned}
&H(C, N, E_{\mathrm{ts}}, E_{\mathrm{os}}, \gamma, \mu_1, \mu_2, \mu_3, \mu_4)\\
&\quad = AC(t) + B\gamma^2(t) + \mu_1\big(-\alpha(C - C_0) + \lambda_1 N + \lambda_2 E_{\mathrm{ts}}\big)\\
&\qquad + \mu_2\left(sN\left(1 - \frac{N}{L}\right) - \theta(C - C_0)N + \beta N\big(\big(1 - \gamma(t)\big)E_{\mathrm{ts}} + \gamma(t)E_{\mathrm{os}}\big)\right)\\
&\qquad + \mu_3\left(\frac{k_1(1 - \gamma(t))NE_{\mathrm{ts}}}{m + N} - \gamma_{\mathrm{ts}}E_{\mathrm{ts}}^2\right) + \mu_4\left(\frac{k_2\gamma(t)NE_{\mathrm{os}}}{m + N} - \gamma_{\mathrm{os}}E_{\mathrm{os}}^2\right).
\end{aligned}$$

Here μ_i $(i = 1, 2, 3, 4)$ are adjoint variables.

The optimality system is

$$\begin{aligned}
&\dot{C} = -\alpha(C - C_0) + \lambda_1 N + \lambda_2 E_{\mathrm{ts}},\\
&\dot{N} = sN\left(1 - \frac{N}{L}\right) - \theta(C - C_0)N + \beta N\big(\big(1 - \gamma(t)\big)E_{\mathrm{ts}} + \gamma(t)E_{\mathrm{os}}\big),\\
&\dot{E_{\mathrm{ts}}} = \frac{k_1(1 - \gamma(t))NE_{\mathrm{ts}}}{m + N} - \gamma_{\mathrm{ts}}E_{\mathrm{ts}}^2, \qquad \dot{E_{\mathrm{os}}} = \frac{k_2\gamma(t)NE_{\mathrm{os}}}{m + N} - \gamma_{\mathrm{os}}E_{\mathrm{os}}^2,
\end{aligned}$$

$$
\begin{aligned}
\dot{\mu_1} &= -A + \mu_1\alpha + \mu_2\theta N,\\
\dot{\mu_2} &= -\mu_1\lambda_1 - \mu_2\left(s\left(1-\frac{2N}{L}\right) - \theta(C-C_0) + \beta\big\{(1-\gamma)E_{\rm ts} + \gamma E_{\rm os}\big\}\right)\\
&\quad - \mu_3\frac{k_1(1-\gamma)mE_{\rm ts}}{(m+N)^2} - \mu_4\frac{k_2\gamma mE_{\rm os}}{(m+N)^2},\\
\dot{\mu_3} &= -\mu_1\lambda_2 - \mu_2\beta(1-\gamma)N - \mu_3\left\{\frac{k_1(1-\gamma)N}{m+N} - 2\gamma_{\rm ts}E_{\rm ts}\right\},\\
\dot{\mu_4} &= -\mu_2\beta\gamma N - \mu_4\left\{\frac{k_2\gamma N}{m+N} - 2\gamma_{\rm os}E_{\rm os}\right\},
\end{aligned}
$$

here $C(0) \geqslant C_0$, $N(0) \geqslant 0$, $E_{\rm ts}(0) \geqslant 0$, $E_{\rm os}(0) \geqslant 0$, $\mu_i(t_f) = 0$, and the optimal control γ^*, which minimizes the functional J subjected to system (12), is given as

$$
\gamma^* = \frac{\mu_2\beta N(E_{\rm ts} - E_{\rm os}) + \frac{\mu_3 k_1 N E_{\rm ts}}{m+N} - \frac{\mu_4 k_2 N E_{\rm os}}{m+N}}{2B}.
$$

4 Numerical simulation

To validate the analytical results and understand the dynamics of model (1), we conduct numerical simulations using the parameter values listed in Table 1. Values of some of the parameters are taken from the study done by Verma et al. [29], other are considered to capture the whole dynamics of the proposed model and are biologically meaningful. For the considered set of parameter values, the components of interior equilibrium E^* and corresponding eigenvalues are calculated as

$$
\begin{aligned}
&C^* = 372.12, \quad N^* = 665.23, \quad E^*_{\rm ts} = 30.38, \quad E^*_{\rm os} = 37.13,\\
&-0.0037, \quad -0.0070, \quad -0.0163 + 0.0074{\rm i}, \quad -0.0163 - 0.0074{\rm i}.
\end{aligned}
$$

The eigenvalues confirm that the equilibrium E^* is locally asymptotically stable as all eigenvalues have negative real parts. Furthermore, the parameter values in Table 1 satisfy the conditions for the global stability of equilibrium E^* as outlined in Theorem 2. Moreover, Fig. 1 shows that solution trajectories from any initial point within the region of attraction converge to E^* in the NC-plane, depicting the global stability of E^*.

Table 1. Values assigned to the parameters for numerical simulations.

Parameter	Value	Source	Parameter	Value	Source
α	0.01612	Ref. [29]	λ_1	0.001	assumed
β	0.00001	assumed	s	0.0265	Ref. [29]
θ	0.0001	assumed	C_0	280	Ref. [29]
$\gamma_{\rm ts}$	0.0002	assumed	$\gamma_{\rm os}$	0.0001	assumed
k_1	0.02	assumed	k_2	0.01	assumed
λ_2	0.02698	Ref. [29]	L	1000	Ref. [29]
γ	0.55	assumed	m	320	Ref. [29]

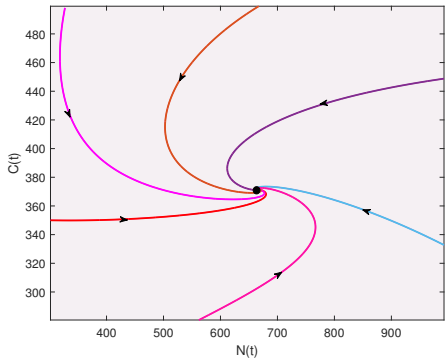

Figure 1. Global stability of E^* in NC-plane (trajectories with distinct initial starts are shown by different colors).

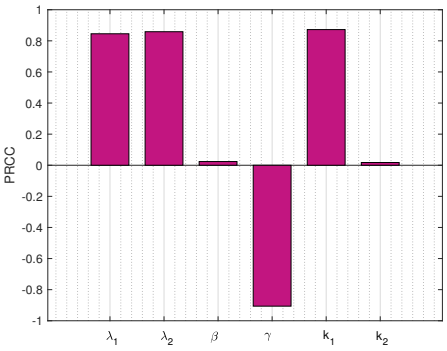

Figure 2. Effect of uncertainty of parameters λ_1, λ_2, β, γ, k_1, and k_2 on $C(t)$.

4.1 Sensitivity of parameters

In accordance with Marino et al. [16], we address the uncertainties associated with selecting parameter values in the system represented by Eq. (1). To account for the variability in our parameters of interest, λ_1, λ_2, β, γ, k_1, and k_2, we conduct 10,000 simulations of the model system (1) using LHS approach. In this approach, we assume a uniform distribution for these parameters and allow them to vary within $\pm 50\%$ of their nominal values, which are provided in Table 1. This methodology helps us to mitigate the uncertainties inherent in parameter selection. The PRCC values using the atmospheric CO_2 as a response function are shown in Fig. 2. The figure shows that the parameter γ is inversely related to the concentration of atmospheric CO_2, and the parameters λ_1, λ_2, β, k_1, and k_2 have positive correlations. This analysis demonstrates that among all these considered parameters, the parameters γ, k_1, and λ_2 are the most influential parameters subjected to the atmospheric CO_2 for the parameter values chosen in Table 1.

To examine the combined impact of the parameters k_1 and γ on the equilibrium level of atmospheric CO_2, a plot is presented in Fig. 3(a). The figure demonstrates that when the fraction of human dependency on renewable energy sources (parameter γ) is held constant, an increase in parameter k_1 leads to higher atmospheric CO_2 level. This occurs because greater reliance on traditional energy sources results in increased fossil fuel combustion, which elevates CO_2 emissions. Conversely, if k_1 is kept constant while increasing the reliance on renewable energy sources, the atmospheric CO_2 level decreases. Further, Fig. 3(b) shows the values of C^* and N^* for several values of λ_2. This figure demonstrates that as the value of λ_2 increases, the atmospheric level of CO_2 increases and the human population decreases in the considered region. Furthermore, this decrease in human population leads to a decrease in energy demand. Figure 3(a) illustrates how increasing reliance on traditional energy sources leads to higher CO_2 level, while a shift towards renewable energy mitigates these emissions. This finding emphasizes the potential of renewable energy in controlling atmospheric CO_2. Similarly, Fig. 3(b)

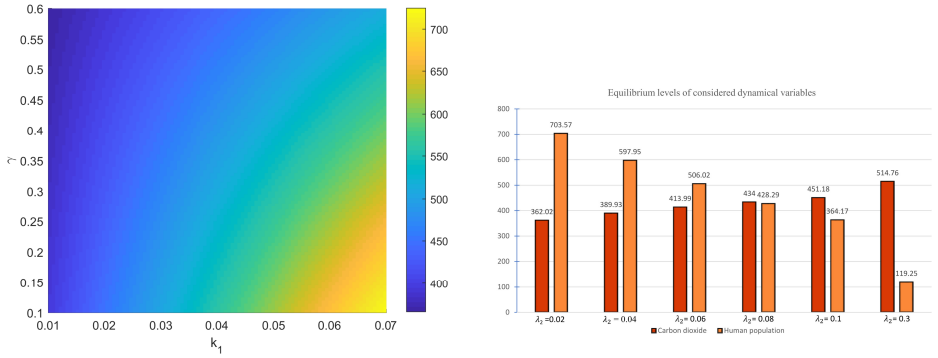

(a) (b)

Figure 3. (a) Combined effect of parameters k_1 and γ on C^*. (b) Bar diagram showcasing the values of C^* and N^* for different values of λ_2.

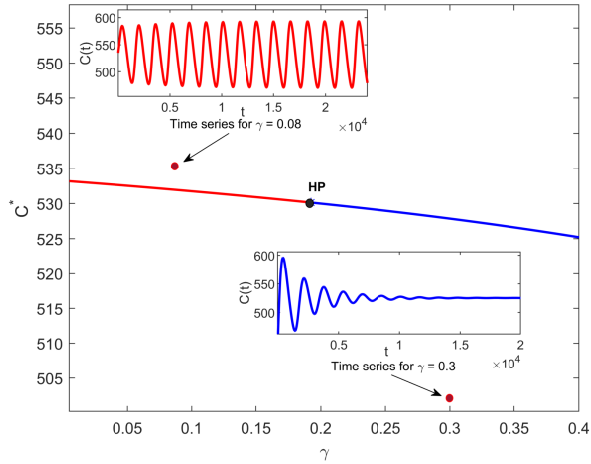

Figure 4. Hopf bifurcation concerning parameter γ with all the parameter values as considered in Table 1 and $\alpha = 0.0016$.

demonstrates the relationship between increased energy production through conventional sources, higher CO_2 level, and their adverse effects on human population.

Varying the parameter γ causes the model system (1) to undergo Hopf bifurcation. Equilibrium E^* is unstable for low values of γ, and as γ exceeds a critical value, the system becomes stable through Hopf bifurcation. Figure 4 illustrates the equilibrium level of CO_2 for different values of γ. This figure demonstrates that system (1) undergoes Hopf bifurcation at $\gamma = 0.1924$ (say γ_c, shown by HP in mentioned figure). The phase portrait (shown in Fig. 5(a)) illustrates that for lower values of $\gamma = 0.08$ ($< \gamma_c$), both the solution trajectories approach to the limit cycle. This indicates that the solution trajectories will oscillate periodically over time. On the other hand, for $\gamma = 0.3 > \gamma_c$, the solution trajectory is approaching its equilibrium level, i.e., instead of showing oscillatory dynamics,

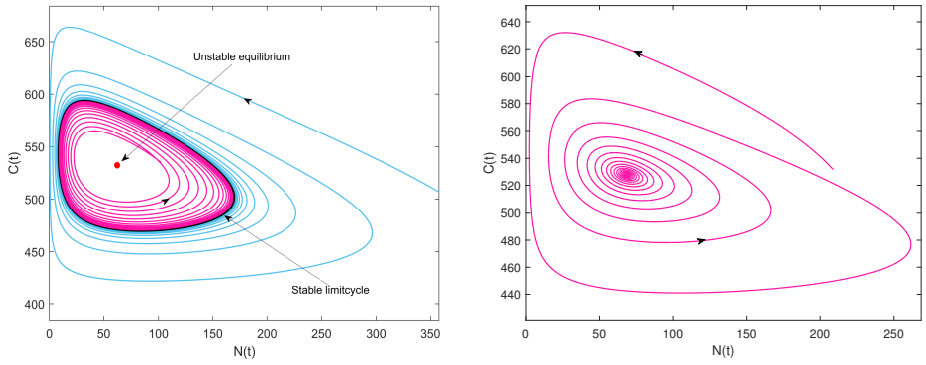

(a) $\gamma = 0.08$ (b) $\gamma = 0.3$

Figure 5. Phase portrait for $\gamma = 0.08, 0.3$. Here all parameters are same as in Table 1 except $\alpha = 0.0016$.

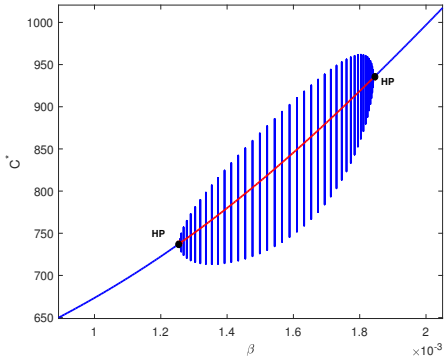

Figure 6. Bubbling phenomenon concerning parameter β with all the parameter values as considered in Fig. 4 except $\gamma = 0.5$.

the solution trajectory will stabilize at a fixed level shown in Fig. 5(b). The physical significance of this phenomenon is that when the proportion of energy generated from renewable sources is small, energy production from traditional sources increases along with a rise in CO_2 emissions. This results in higher level of atmospheric CO_2. Further, due to its adverse impacts, the human population will decline. This decline in population results to lower energy demand, hence the atmospheric CO_2 will reduce, and this results in higher density of human population. Thus, an oscillatory dynamics will be observed for lower values of γ. However, when the value of γ crosses a threshold level, i.e., human population depends more on renewable energy sources, then the atmospheric CO_2 and all the dynamical variables reach to stable equilibrium levels. Thus, Fig. 4 demonstrates how the system experiences Hopf bifurcation at a critical threshold ($\gamma = 0.1924$), transitioning from oscillatory to stable dynamics as γ increases. This bifurcation signifies a shift from periodic fluctuations in CO_2 level and population density to stable equilibrium due to increased reliance on renewable energy. Furthermore, the phase portraits in Figs. 5(a) and 5(b)provide a visual representation of this behavior. For $\gamma < \gamma_c$, oscillatory trajectories

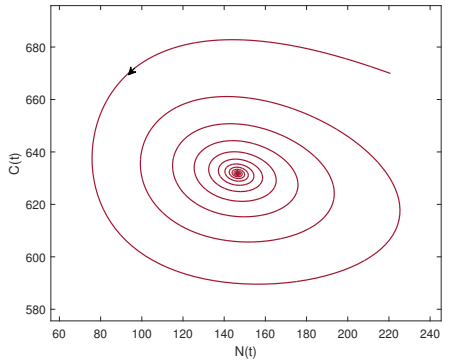

(a) $\beta = 0.0008$

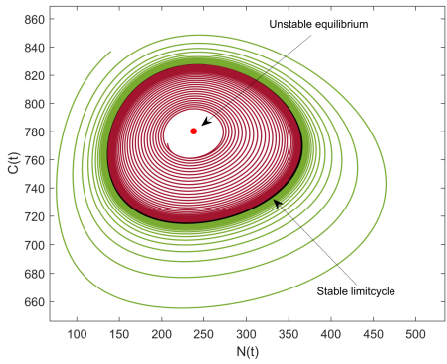

(b) $\beta = 0.0014$

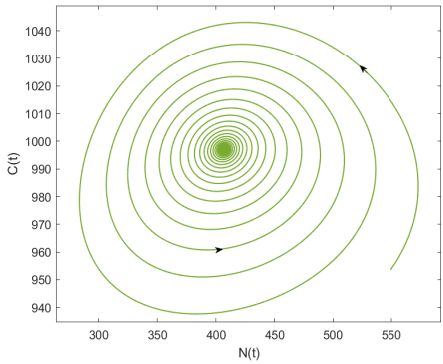

(c) $\beta = 0.002$

Figure 7. Phase portrait for (a) $\beta = 0.0008, 0.0014, 0.002$. Here all parameters are same as in Table 1 except $\alpha = 0.0016$.

(limit cycles) dominate, reflecting the interplay between population and energy demand. For $\gamma > \gamma_c$, the trajectories stabilize at equilibrium, indicating a balance achieved through higher renewable energy use.

Furthermore, we observed that the model system described by Eq. (1) experiences a Hopf bifurcation concerning the parameter β. Notably, this parameter β triggers a bubbling phenomenon in the system; see Fig. 6. From this figure, we may note that the critical level of β at first Hopf-point is obtained as $\beta_{c_1} = 0.001257$. At this point, i.e., $\beta_{c_1} = 0.001257$, periodic oscillations generate. Moreover, the oscillatory dynamics die out and the formulated system gains its stability at $\beta_{c_2} = 0.001841$. Further, Fig. 7(a) depicts that the solution trajectory approaching the interior equilibrium E^* for $\beta = 0.0008 < \beta_c$. In Fig. 7(b), for $\beta = 0.0014$ (where $\beta_{c_1} < \beta = 0.0014 < \beta_{c_2}$), the trajectory repels from the interior equilibrium, with all solutions, whether starting inside or outside the limit cycle, moving towards it. Figure 7(c) for $\beta = 0.002$ demonstrates stable atmospheric CO_2 behavior as $\beta = 0.002 > \beta c_2$. These figures demonstrate the significance of the parameter β in driving the system's transition through bifurcation points, leading to oscillatory

dynamics at β_{c_1} and stability at β_{c_2}. This highlights how β influences CO_2 stabilization and periodic behavior, provides insights into critical thresholds for system stability.

4.2 Simulation results regarding optimal control

Forward-backward sweep method is used to solve the optimality system (12) [14]. The optimal system is solved for the set of parameter values mentioned in Table 1. We have considered the maximum value of γ as $\gamma_{\max} = 0.7$ and the values of weight constants as $A = 1$ and $B = 3$. The values of weight constants are chosen only for the illustration of theoretically obtained results. In Fig. 8(a), we have plotted the atmospheric concentration of CO_2 for 30 years with and without implementation of control strategies for mentioned values of $\gamma_{\max}$ and weight constants. Figure 8(a) illustrates that in the absence of considered control strategy, the atmospheric level of CO_2 attains a level of 375.9 ppm, and by the implementation of considered control strategy, it reduces to 362.9 ppm. Moreover, we have plotted the optimal control profile in Fig. 8(b) for considered values of weight constants and $\gamma_{\max}$. From this figure it can be illustrated that the dependency of human population on renewable energy sources increases to its maximum attainable growth rate till 10.7 years than it can be reduced.

In Fig. 9(a), we have plotted the optimal profiles for two different values of maximum attainable rate of dependency of human population on renewable energy sources. Here we have considered weight constants same as above and varied the value of $\gamma_{\max}$ as $\gamma_{\max} = 0.7$ and $\gamma_{\max} = 0.9$. In case of $\gamma_{\max} = 0.9$, the dependency of human population on renewable energy sources must be maximum for 5 years, which was 10.7 years for $\gamma_{\max} = 0.7$. Further, we have generated the optimal profiles for two different values of weight constants in Fig. 9(b). We have considered weight constants as $A = 1$, $B = 3$ and $A = 1$, $B = 4$, here we have increased the value of B, i.e., in this case, more emphasis is given on increasing the dependency of human population on renewable sources of

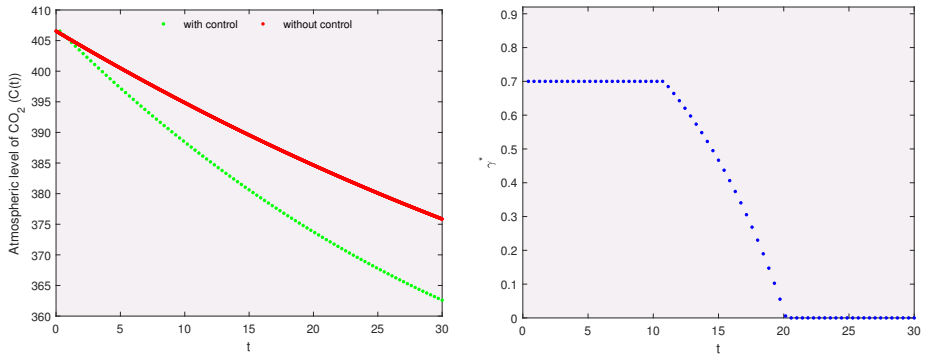

(a) (b)

Figure 8. (a) Projection of atmospheric level of CO_2 with and without optimal control. (b) Optimal profile of control variable γ. Here $A = 1$, $B = 3$, $\gamma = 0.5$, and $\gamma_{\max} = 0.7$.

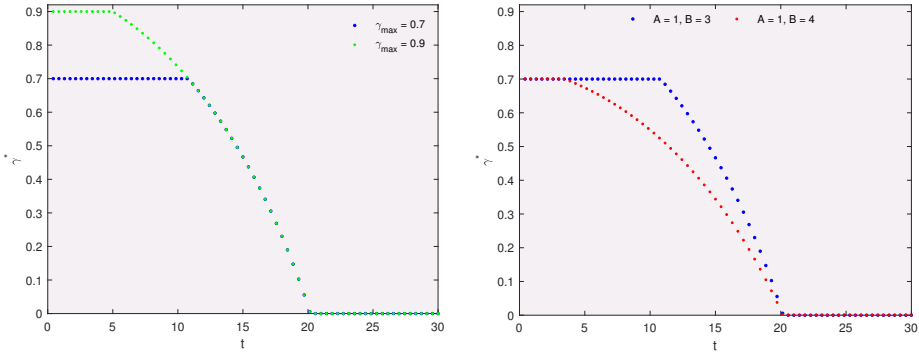

(a) (b)

Figure 9. Optimal profiles of control variable γ^* for different values of (a) $\gamma_{\max}$ and (b) weight constants with all parameters same as in Table 1 except $\gamma = 0.5$.

energy. This figure depicts that for $A = 1$, $B = 4$, the implementation of considered strategy must be done with maximum attainable rate till 3.5 years, and after that, it can be reduced. This obtained scenario illustrates that for higher values of weight constant B, the year of implementation of considered strategy with maximum rate decreases significantly. These figures illustrate the effectiveness of the proposed control strategies in reducing atmospheric CO_2 level and optimizing dependency on renewable energy. Without control, CO_2 reaches 375.9 ppm, but with control, it decreases to 362.9 ppm. The optimal control profiles show that higher maximum dependency rates ($\gamma_{\max}$) and increased emphasis on renewable energy (higher B) reduce the duration for which maximum implementation is required, highlights the importance of tailored strategies for CO_2 mitigation.

5 Conclusion

This research presents a nonlinear mathematical model to examine the effects of transitioning energy production from conventional energy sources to clean energy sources on atmospheric CO_2 dynamics. The model explicitly incorporates variables representing energy demand from coal, oil, gas, and renewable sources. The stability theory for differential equations was applied to analyze the system, and numerical simulations were conducted with specific parameter values to support the analytical results and explore additional dynamics.

The analysis identified conditions holding which the system's coexisting equilibrium is locally and globally stable. It was observed that human population growth, driven by energy consumption, destabilizes the system by increasing anthropogenic CO_2 emissions. Furthermore, the system experiences a Hopf bifurcation around the coexisting equilibrium when the population's reliance on renewable energy sources drops below a critical threshold, leading to instability and periodic oscillations. These findings highlight the risk of uncontrolled increases in traditional energy use, whereas greater reliance on renewable sources stabilizes the system and reduces oscillations. The results demonstrate that

a higher dependency on renewable energy enables the atmospheric CO_2 level to stabilize and even decrease over time. A sensitivity analysis using the PRCC method revealed that dependence on renewable energy is the key factor influencing CO_2 dynamics. Other important factors include the growth in energy demand from traditional sources and the CO_2 emission rate resulting from fossil fuel combustion. Additionally, an optimal control approach following Pontryagin's maximum principle was implemented to minimize both atmospheric CO_2 level and the associated costs. The results showed that increasing renewable energy production growth reduces the duration for which mitigation strategies need to be applied, effectively lowering CO_2 level compared to scenarios without such strategies.

This research also examines the impact of per capita energy demand from renewable and nonrenewable sources on atmospheric CO_2. While the study is preliminary and relies on simplified assumptions, the findings can be validated using real-world data by calibrating the model parameters with observed values. Policymakers can use these insights to develop strategies addressing rising energy demands and reducing CO_2 emissions. The study emphasizes that promoting a transition to renewable energy is a viable solution for controlling atmospheric CO_2 concentrations, avoiding oscillatory behavior and achieving climate change targets. By encouraging this shift, the research aims to inform policy development and support efforts to mitigate carbon emissions and combat climate change.

References

1. B. Bhandari, S.R. Poudel, K.-T. Lee, S.H. Ahn, Mathematical modeling of hybrid renewable energy system: A review on small hydro-solar-wind power generation, *Int. J. Pr. Eng. Man.-G. Technol.*, **1**:157–173, 2014, https://doi.org/10.1007/s40684-014-0021-4.
2. S. Bilgen, K. Kaygusuz, A. Sari, Renewable energy for a clean and sustainable future, *Energy Sources*, **26**(12):1119–1129, 2004, https://doi.org/10.1080/00908310490441421.
3. S.R. Bull, Renewable energy today and tomorrow, *Proc. IEEE*, **89**(8):1216–1226, 2001, https://doi.org/10.1109/5.940290.
4. M.A.L. Caetano, D.F.M. Gherardi ans T. Yoneyama, An optimized policy for the reduction of CO_2 emission in the Brazilian Legal Amazon, *Ecol. Model.*, **222**(15):2835–2840, 2011, https://doi.org/10.1016/j.ecolmodel.2011.05.003.
5. S. Devi, N. Gupta, Effects of inclusion of delay in the imposition of environmental tax on the emission of greenhouse gases, *Chaos Solitons Fractals*, **125**:41–53, 2019, https://doi.org/10.1016/j.chaos.2019.05.006.
6. I. Dincer, Environmental issues: II-potential solutions, *Energy Sources*, **23**(1):83–92, 2001, https://doi.org/10.1080/00908310151092218.
7. B. Dubey, A. Kumar, Dynamics of prey–predator model with stage structure in prey including maturation and gestation delays, *Nonlinear Dyn.*, **96**(2):2653–2679, 10.1007/s11071-019-04951-5, https://doi.org/2019.
8. X. Fan, X. Li, J. Yin, Impact of environmental tax on green development: A nonlinear dynamical system analysis, *PLoS One*, **14**(9):e0221264, 2019, https://doi.org/10.1371/journal.pone.0221264.

9. H.I. Freedman, J.W.H. So, Global stability and persistence of simple food chains, *Math. Biosci.*, **76**:69–86, 1985, https://doi.org/10.1016/0025-5564(85)90047-1.

10. L.C. Grobusch, M.P. Grobusch, A hot topic at the environment–health nexus: Investigating the impact of climate change on infectious diseases, *Int. J. Infect. Dis.*, **116**:7–9, 2022, https://doi.org/10.1016/j.ijid.2021.12.350.

11. I. Hanif, S.M.F. Raza, P. Gago de Santos, Q. Abbas, Fossil fuels, foreign direct investment, and economic growth have triggered CO_2 emissions in emerging Asian economies: Some empirical evidence, *Energy*, **171**:493–501, 2019, https://doi.org/10.1016/j.energy.2019.01.011.

12. T.M. Harris, J.P. Devkota, V. Khanna, P.L. Eranki, A.E. Landis, Logistic growth curve modeling of US energy production and consumption, *Renewable Sustainable Energy Rev.*, **96**: 46–57, 2018, https://doi.org/10.1016/j.rser.2018.07.049.

13. K. Lata, A.K. Misra, Modeling the effect of economic efforts to control population pressure and conserve forestry resources, *Nonlinear Anal. Model. Control*, **22**(4):473–488, 2017, https://doi.org/10.15388/NA.2017.4.4.

14. S. Lenhart, J.T. Workman, *Optimal Control Applied to Biological Models*, Chapman & Hall/CRC, New York, 2007, https://doi.org/10.1201/9781420011418.

15. Z.N. Lu, H. Chen, Y. Hao, J. Wang, X. Song, T.M. Mok, The dynamic relationship between environmental pollution, economic development and public health: Evidence from China, *J. Cleaner Prod.*, **166**:134–147, 2017, https://doi.org/10.1016/j.jclepro.2017.08.010.

16. S. Marino, I.B. Hogue, C.J. Ray, D.E. Kirschner, A methodology for performing global uncertainty and sensitivity analysis in systems biology, *J. Theor. Biol.*, **254**(1):178–196, 2008, https://doi.org/10.1016/j.jtbi.2008.04.011.

17. B. Metz, O. Davidson, P. Bosch, R. Dave, L. Meyer, Mitigation of climate change, Contribution of working group ii to the fourth assessment report of the intergovernmental panel on climate change (ipcc), 2007.

18. A.K. Misra, Modeling the depletion of dissolved oxygen in a lake due to submerged macrophytes, *Nonlinear Anal. Model. Control*, **15**(2):185–198, 2010, https://doi.org/10.15388/NA.2010.15.2.14353.

19. A.K. Misra, A. Jha, Modeling the effect of population pressure on the dynamics of carbon dioxide gas, *J. Appl. Math. Comput.*, **67**(1–2):623–640, 2021, https://doi.org/10.1007/s12190-020-01492-8.

20. A.K. Misra, A. Jha, Modeling the effect of budget allocation on the abatement of atmospheric carbon dioxide, *Comput. Appl. Math.*, **41**(5):202, 2022, https://doi.org/10.1007/s40314-022-01906-2.

21. A.K. Misra, A. Jha, How to combat atmospheric carbon dioxide along with development activities? A mathematical model, *Physica D*, **454**:133861, 2023, https://doi.org/10.1016/j.physd.2023.133861.

22. A.K. Misra, M. Verma, Impact of environmental education on mitigation of carbon dioxide emissions: A modelling study, *Int. J. Global Warming*, **7**(4):466–486, 2015, https://doi.org/10.1504/IJGW.2015.070046.

23. A. Mostafaeipour, A. Bidokhti, M.-B. Fakhrzad, A. Sadegheih, Y.Z. Mehrjerdi, A new model for the use of renewable electricity to reduce carbon dioxide emissions, *Energy*, **239**(A): 121602, 2022, https://doi.org/10.1016/j.energy.2021.121602.

24. M. Nadeem, M. Habib, M. Safdar, P.K. Mwanakatwe, Y. Gurefe, Analysis of climatic model using fractional optimal control, *J. Math.*, **2023**:1–9, 2023, https://doi.org/10.1155/2023/7482381.

25. A. Sieminski, International energy outlook 2013, Report DOE/EIA-0484, US Energy Information Administration (EIA).

26. R.E. Sims, Bioenergy to mitigate for climate change and meet the needs of society, the economy and the environment, *Mitig. Adapt. Strat. Glob. Chang.*, **8**(4):349–370, 2003, https://doi.org/10.1023/B:MITI.0000005614.51405.ce.

27. P.K. Tiwari, R.K. Singh, D. Jana, Y. Kang, A.K. Misra, A nonautonomous mathematical model to assess the impact of algae on the abatement of atmospheric carbon dioxide, *Int. J. Biomath.*, **14**(7):2150059, 2021, https://doi.org/10.1142/S1793524521500595.

28. M. Verma, A.K. Misra, Optimal control of anthropogenic carbon dioxide emissions through technological options: A modeling study, *Comput. Appl. Math.*, **37**(1):605–626, 2018, https://doi.org/10.1007/s40314-016-0364-2.

29. M. Verma, A.K. Verma, A.K. Misra, Mathematical modeling and optimal control of carbon dioxide emissions from energy sector, *Environ. Dev. Sustainability*, **23**(9):13919–13944, 2021, https://doi.org/10.1007/s10668-021-01245-y.

30. Editorial, *Renewable Energy World*, **6**(6), 2003.

31. IRENA (2018), Global Energy Transformation: A roadmap to 2050, Technical report, International Renewable Energy Agency, Abu Dhabi, 2018.

32. United Nations Environment Programme (UNEP), Emission Gap Report, Nairobi, 2019, http://www.unenvironment.org/emissionsgap.